COMMERCIAL MESOPOROUS ZEOLITE-SUPPORTED TITANIUM OXIDE FOR THE PHOTOCATALYTIC DEGRADATION OF PHARMACEUTICAL POLLUTANTS

M.W. Ibrahim[1], R.Y. Ghazal[1*], H.Y. Ridha[1], H. Kosslick[2] and A. Schulz[2]

[1]*Department of Chemistry, College of Pure Science, University of Mosul, Mosul, Iraq*
[2]*Department of Inorganic Chemistry, Institute of Chemistry, University of Rostock, Rostock, Germany*
**e-mail: ragheedghazal76@uomosul.edu.iq*

Received 25.07.2025
Accepted 05.11.2025

Abstract: *The current research aims to evaluate the photocatalytic activity of (TiO_2) with various loading ratios (5%-60%) supported on mesoporous aluminosilicate (zeolite type) called Siral, with aluminum content ranging from 20% to 70%, to enhance the performance of degradation of ibuprofen (IBP) as a pharmaceutical pollutant. The batch reactor is furnished with solarium light to simulate sunlight UV for efficient degradation. The supported substance (Siral) exhibits elevated surface area and a regular mesoporous structure; hence, it might be regarded as an efficient photocatalyst support. The characterizations and effectiveness of the prepared catalyst were achieved by X-ray diffraction (XRD), Brunauer-Emmett-Teller (BET), scanning electron microscopy (SEM) and UV-visible spectroscopy. The results exhibit the highest photo-degradation ratio (90%) for (60% TiO_2/Siral40) after 4 hours. The highest surface area is 448.3685 m^2/g for 15% TiO_2/Siral40. The photodegradation efficiency increases as the weight percentage of TiO_2 particles rises from 5 to 60 %. TiO_2/Siral NCs photocatalysts demonstrate remarkable photostability and reusability, especially in organic molecule degradation.*

Keywords*: Titanium dioxide, Ibuprofen, Photodegradation, Siral, Pollution.*

1. Introduction

Zeolite and Siral groups are mesoporous aluminosilicate materials with excellent adsorption, ion exchange capacity, and suitable surface area [1, 2] . Thereby, loading of TiO_2 as an oxidative substance on the aluminosilicate surface provides selectively moderate pore catalysts that can degrade organic molecules [3].

However, because the specifications of these materials are difficult, little is known about the arrangement of Si, Al, and O in the aluminosilicate at different scales. Silica-alumina combinations have high-temperature patience and good stability for prolonged reaction times [4]. Fig. 1 illustrates the diverse mixing of (Sasol Boehmite) SB-type alumina and silica to form different percentages of aluminosilicate.

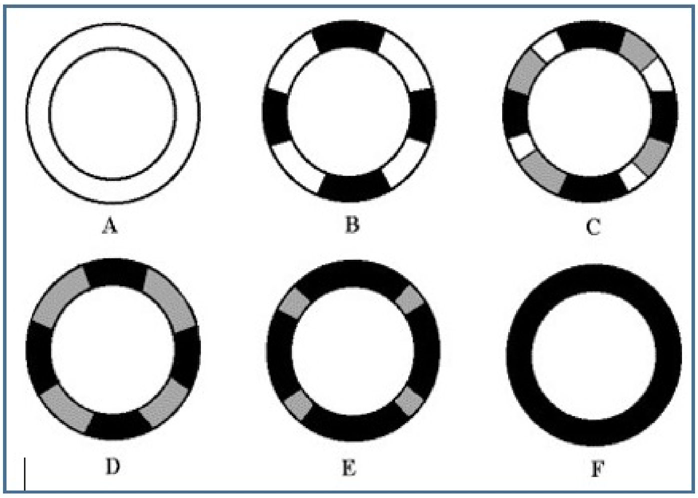

Fig. 1. Exterior formation: SB (A), (SB:SIRALs 1:1.5–5) (B), (SB:SIRALs 1:10–20) (C), (SB:SIRALs 1:30–40) (D), (SB:SIRALs 1:60–80) (E) and SIRALs 90–100 (F) [1, 5]

As a result of the rapid increase in industrial growth and urban development, water is becoming more polluted and contaminated than ever before by various toxins that pollute drinking water, such as pharmaceuticals, solvents, insecticides, oils, and coloring substances. These materials produce a large amount of harmful and persistent substances due to their widespread use in various industries and cannot be easily removed [6]. The increasing request for clean and safe water appropriate for human use needs to develop techniques for the treatment of wastewater because pure water is a life essence for all living organisms [7].

A few customary strategies are created for the medication of industrial drainage, but advanced oxidation forms were viewed as the most effective ones. These days, radicals of hydroxyl (•OH) have been used to increase the degradation of natural debasements into the least harmful. By using catalysts, the technique is to change poisonous materials into non-poisonous ones [8, 9].

Among the obstacles to the photocatalytic process is powerless adsorption. To overcome this issue, an adsorbent can act as a supporting material for the photocatalyst [10]. Albiss and Abu-Dalo et al. (2021) are investigating the combination of a ZnO photocatalyst and activated charcoal to degrade methylene blue dye [11].

TiO_2 P25 (Phase 25nm) is still widely used for its high effectiveness and low cost [12]. The degradation of organic and pharmaceutical compounds in water can be improved by combining TiO_2 with zeolite, as was examined. Using TiO_2 as a degradation substance is due to the formation of radicals to oxidize these pollutants in particular conditions of ultraviolet irradiation [13]. The improvement is clarified by the adsorption of pollutants, or partially decayed pollutants, on the zeolite surface, which increases the concentration of the pollutants within the vicinity of the TiO_2 semiconductor and increases the photo-catalytic reaction rate [14].

In the presence of ultraviolet light, TiO_2's semiconductor properties cause an electron (e^-) to jump to the conduction ion band after it was in the valence band. This leads to the generation of positive holes (h^+) at electron sites, which lead to the formation of hydroxyl ($OH^\cdot$) and superoxide ($O_2^{\cdot -}$) radicals that can oxidize organic pollutants in water; hence, these organic molecules will be degraded [15]. Understanding the oxidation process requires knowledge of the mechanism and intermediates [16]. Considering this viewpoint, Wang Z. et al. studied the mechanism of TiO_2 and other catalysts practiced in the ibuprofen photodegradation that utilized UV/LED light. Higher photodegradation was noticed in acidic media. Photocatalysts, including TiO_2, are faster and more effective when compared to some catalysts such as hydrogen peroxide (H_2O_2), $K_2S_2O_8$, and $KHSO_5$. Hydroxyl radicals are generated by H_2O_2 during the photodegradation reaction; the percentage of degradation reached 38.93%, while when using TiO_2 reached 100% [17].

Previous studies have confirmed the ability of this type of photocatalyst in this research route. Miranda et al. investigate the photodegradation mechanism of ibuprofen; three radicals are generated in this process ($OH^\cdot$, $O_2^{-\cdot}$, and $OOH^\cdot$), but the hydroxyl radical has a higher degradation ability compared with other radicals; it attacks the aromatic ring in ibuprofen. The degradation ratio reached 100% [18].

Gayathri et al. used TiO_2/H-Beta zeolite (THB) as a photocatalyst for caffeine degradation. The as-prepared THB composite exhibited outstanding activity for the breakdown of a 10 ppm caffeine solution, according to photocatalytic experiments [19]. Diban et al. combined the photocatalyst TiO_2 with zeolite Y (ZY) to increase the porosity and activity for use in the degradation of organic pollutants. The results indicate that photocatalytic activity is maintained in the physical combination of zeolite and TiO_2 [8]. Mergenbayeva et al. prepared two types of composite photocatalysts (TiO_2 loaded with zeolite 45 and Zeolite Socony Mobil-5 (ZSM-5) for the degradation of the antibiotic pollutant sulfamethoxazole in water using a UV source. The results show complete degradation of the pollutant in 10 minutes [20]. Wang Y. et al. enhanced the rheological specifications of asphalt using Nano-TiO_2 as a photocatalyst binder with graphite/carbon nitride C_3N_4, Based on the results, TiO_2-modified asphalt outperformed C_3N_4-modified asphalt in terms of rutting resistance and outstanding rheological characteristics [21, 22]. The current research aims to investigate the ability of prepared photocatalysts (TiO_2/Siral) in different ratios for the photodegradation of ibuprofen in aqueous solution.

2. Experimental part

2.1. Materials. Ibuprofen sodium salt (IBP-Na) $C_{13}H_{17}NaO_2$ (purity > 98%) Chemical Abstract Service (CAS) Number: 31121-93-4, a non-steroidal anti-inflammatory drug chosen as the model for pollutants from Sigma–Aldrich Co. Titanium oxide (CAS Number: 13463-67-7) is employed as a photocatalyst (Sigma-Aldrich), a white solid, odorless, and insoluble in water. The catalyst was combined with diverse artificial mesoporous aluminosilicate materials as support in a solid situation in a solvent-free procedure. A mortar is used to mill the samples for photocatalytic degradation use. The distilled water is utilized to prepare solutions during the experiments. Amorphous silica-alumina are commercially obtained catalysts from Sasol, Germany.

2.2. Procedures. ***Supporting titanium oxide on Siral***. Various quantities of TiO_2 catalyst are mechanically blended with Siral 20, 30, 40, and 70 with different Al/Si ratios, surface areas, bulk densities, and pore volumes; they have been utilized as supports. The mixtures are ground for fifteen minutes in a ceramic mortar until the mixture is well blended. The subsequent powder is calcined at 500°C for 2 hours with air passage. Accordingly, (5-60%) of supported catalysts (TiO_2) as photocatalysts are loaded over four different types of Siral are investigated. In brief, 10 mg of commercial (TiO_2) is utilized to photodegrade 10 ppm IBP solution, the development of binary-supported catalysts using Siral through wet impregnation and dry physical combing, grinding, and calcination. It has been found that physical mixing produces increased photocatalytic activity based on TiO_2 content while wet impregnation has none [23].

Specification and Analysis of Photocatalyst. X-ray diffraction (XRD) patterns achieved on a powder X-ray diffractometer STADI-P (STOE) utilizing monochromatic Ni-filtered CuKα1 radiation (λ = 1.5406 A), nitrogen adsorption using (BET) determined using an automated device (Sorptomatic), and scanning electron microscopy (SEM) methods (Zeiss Merlin VP Compact) have been applied to determine the structural, crystallization, and morphology of the photocatalyst.

Testing of Photocatalyst effectiveness. The photocatalytic performance was evaluated by examining both adsorption behavior and the reduction in ibuprofen (IBP) concentration under batch conditions. Typically, 250 mL of an aqueous ibuprofen solution (10 ppm) and 10 mg of the photocatalyst were placed in a 250 mL batch reactor beaker. The reactor was then positioned inside a light-impermeable aluminum box equipped with four UV/Vis solarium lamps (Philips Co.), mounted on the upper side. The total lamp power was 60 W, with each bulb rated at 15 W. The lamps primarily simulate the UV portion of sunlight, with additional emission in the visible region of the spectrum [24]. The irradiation intensity was approximately 3.2 $mW \cdot cm^{-2}$. A white LED lamp (Toshiba, 16 W) was used to provide general visible-light illumination in the room. During the photocatalytic experiments, the solution was continuously stirred using a magnetic stirrer to ensure uniform suspension of the catalyst. At predetermined time intervals, aliquots of the reaction mixture were withdrawn using a syringe and filtered through a 0.45 μm polytetrafluoroethylene (PTFE) membrane filter prior to analysis. Adsorption experiments were carried out entirely in the dark to exclude any photochemical effects. The residual concentration of IBP was determined using a UV–Vis spectrophotometer (Varian, Cary WinUV) by monitoring the change in absorbance at 222 nm. The percentage degradation of IBP at different irradiation times was calculated using Eq. (1).

$$Abatement(\%) = \frac{A_0 - A_t}{A_0} x100 \tag{1}$$

A_0 is the initial absorption of ibuprofen, and A_t is the absorption at 222 nm after varying periods of UV/vis exposure. The principle of Per Lambert-Beer, the UV absorbance strength and the drug concentration that has been diagnosed are directly correlated. It is also important to declare that all data is obtained at room temperature.

3. Results and Discussion

3.1. Characterization of the photocatalyst. X-ray diffraction patterns of TiO_2 P25 are shown in Fig. 2; diffraction angles and intensities of reflections are well indexed to the theoretical diffraction patterns of Anatase and Rutile from the Joint Committee on Powder Diffraction Standards (JCPDS) database. The observed relatively broad width, or FWHM, of the peaks confirms the presence of a small crystallite size [25]. Peaks of the rutile pattern are narrower compared to anatase, indicating a higher degree of crystallinity and larger crystallite size (Rutile). It has been noted that P-25 is synthesized in the industrial high-temperature combustion process of $TiCl_4$. Refinement of the pattern to the corresponding theoretical patterns confirms the ratio of ~80/20 for anatase and rutile, respectively [26], and has also confirmed that TiO_2 is a highly crystalline catalyst.

The rutile has a smaller band gap of 3.0 eV or 413 nm than Anatase (3.16 eV or 392 nm) [27]. Chen and Lin (2020) asserted the importance of Rutile in TiO_2 to utilize wide energy in sunlight to excite electrons from the valence band to the conducting band and form electron-hole pairs [28]. TiO_2 can strongly absorb (UV) sunlight equal to 410 nm. The particular surface area (SA) of TiO_2 is 54 m^2/g. Then, the nitrogen adsorption method confirms that TiO_2 has non-porous particles; this is asserted by the slight or no change in nitrogen adsorption of silica when (TiO_2) is not added [29].

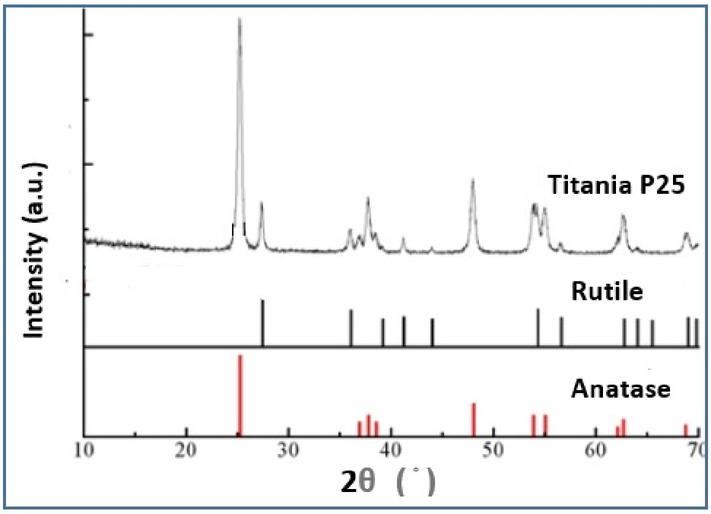

Fig. 2. Powder XRD of Titania (TiO_2 P-25) and corresponding diffraction patterns of Anatase and Rutile

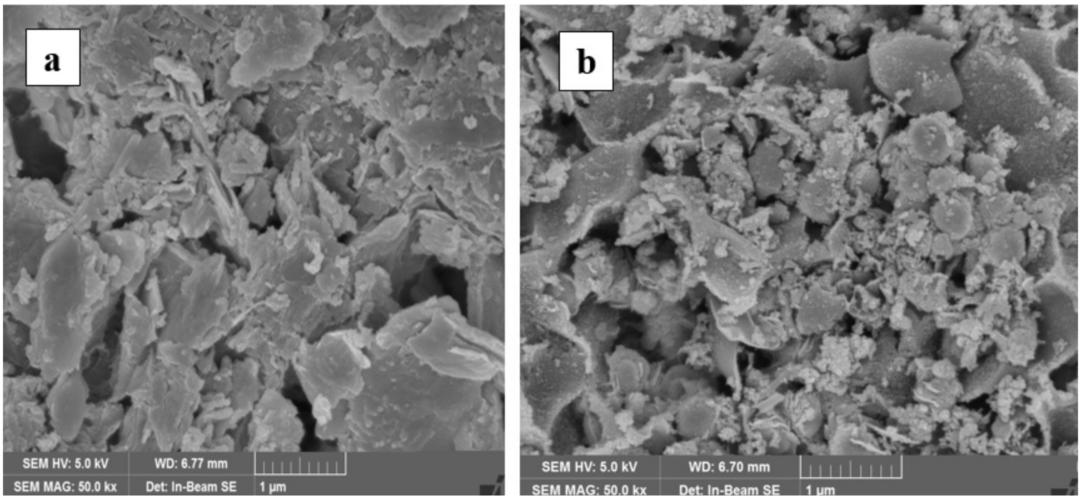

Fig. 3. SEM Images of pure Siral40 (a) and 15%TiO_2/Siral40 (b)

(Fig. 3a) gives information on the morphology of the prepared supports by displaying the FE-SEM of Siral. It is clear from the image that Siral has a smooth surface. In contrast, Siral/TiO_2 NCs

(Fig. 3b) feature granular particles on their unique surface. This validates the existence of TiO_2 particles on Siral's surface. However, the shape of the Siral does not change, suggesting that the presence of TiO_2 particles has not affected the Siral structure.

3.2. TiO_2/Siral composite photocatalytic effectiveness. The well-known finest photocatalyst, Degussa P25 TiO_2, is usually known for its appropriate constituents as a blend of approximately 80% Anatase and 20% Rutile, separately, surpassing the activity of Anatase alone [12]. In the present research, TiO_2/Siral photocatalysts are prepared in several steps: blending, milling, and heating for calcination degree using the identical method discussed in the experimental section. The photodegradation of IBP has been selected as a model of a pollutant in wastewater and used to evaluate the effectiveness of the prepared catalyst under UV irradiation, according to Fig. 4 below:

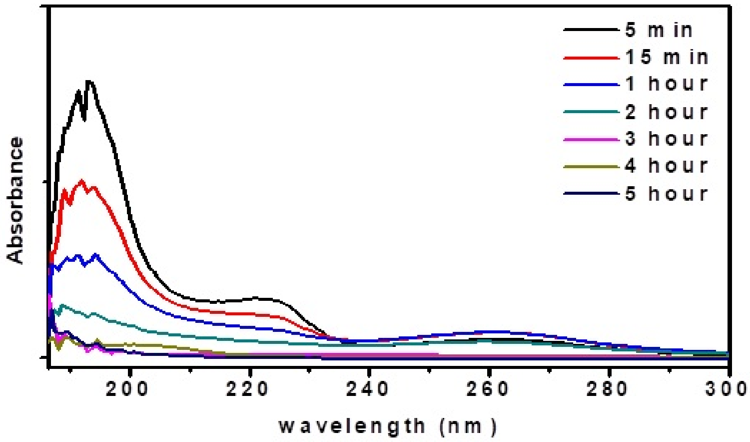

Fig. 4. UV/Vis spectra of treated IBP solution according to time, over (15%TiO_2/Siral 30) Photocatalyst Core-Shell using UV/Vis (10 mg/L catalyst, 250 mL of 10 ppm aqueous IBP, irradiation: 60W UV/Vis light)

We can observe a gradual decline in ibuprofen concentration from Fig. 4. The first hour saw a sharp decline, followed by a slow decline until five hours later, when the concentrations were extremely low. A decline of the phenylene group of IBP absorbance at 193.5 & 222 nm is detected. This is attributed to the degradation of the phenylene group. At the same time, a recent absorbance emerged at 260 nm. The strength of absorbance goes up and down during prolonged treatment. This change in absorbance is ascribed to the creation of intermediates in photocatalytic treatment.

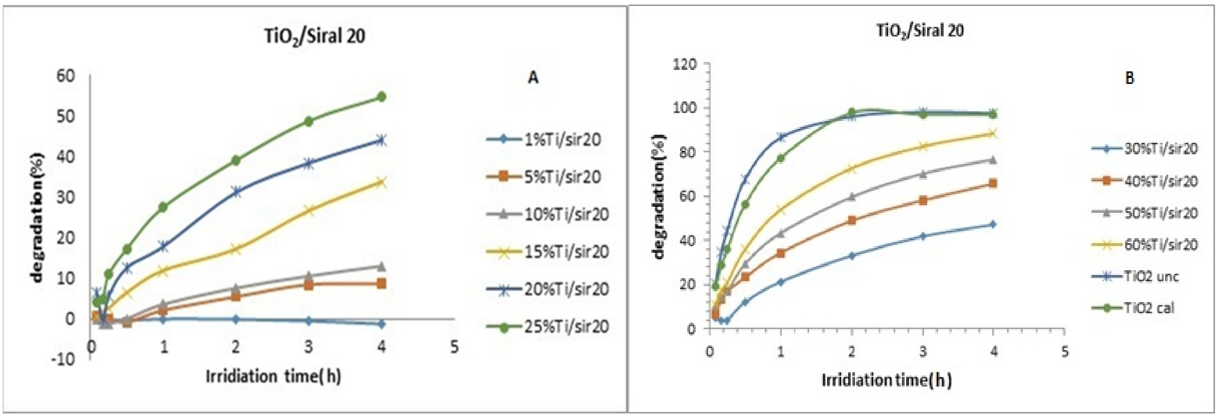

Fig. 5. Photocatalytic decomposition of 4 hours, (a) IBP over (1-25%TiO_2/Siral20) and (b) TiO_2 alone and 30-60%TiO_2/Siral20 with varying catalyst ratios. Conditions: 250 ml batch reactor, ibuprofen conc. (10 ppm), catalyst (10 mg), (4.6 W) UV/Vis, solarium bulb

The photocatalytic efficiency of TiO_2 Degussa begins at the start of the decreasing absorption curve (Fig. 5a). During photocatalytic treatment, there is a significant drop in the concentration of ibuprofen. After 240 min., the ibuprofen concentration decreases by 50% when 25% TiO_2/Sir20 is employed; as the TiO_2 ratio on Sir20 increases, the decrease reaches around 86% when 60% TiO_2/Sir20 is used (Fig. 5b). Treatments with photocatalysts containing 5-50% TiO_2 P-25 show similar photocatalytic efficiency, which increases significantly over 4 hours to 77% with reaction time [30].

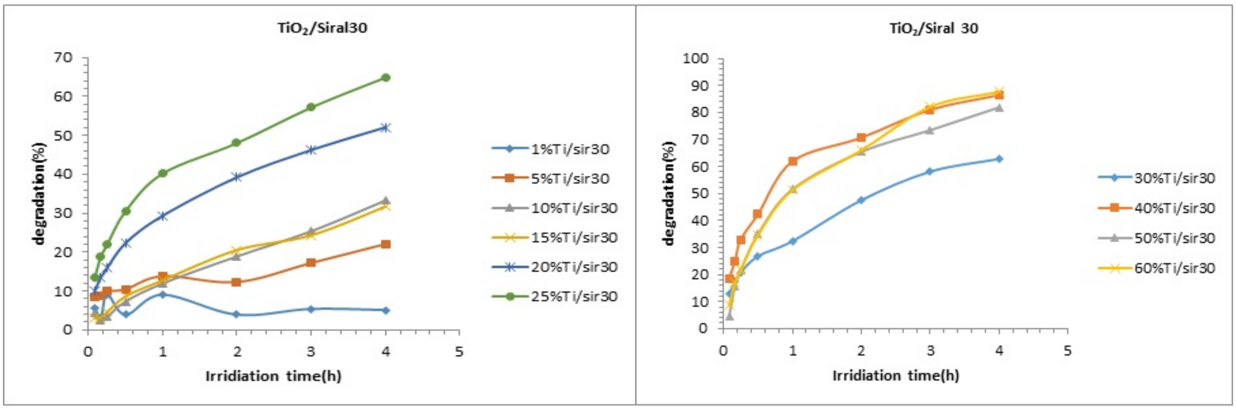

Fig. 6. Photocatalytic decomposition of 4 hours, (a) IBP over (1-25%TiO_2/Siral30) and (b) TiO_2 alone and 30-60%TiO_2/Siral30 with varying catalyst ratios. Conditions: 250 ml batch reactor, ibuprofen conc. (10 ppm), catalyst (10 mg), (4.6 W) UV/Vis, solarium bulb

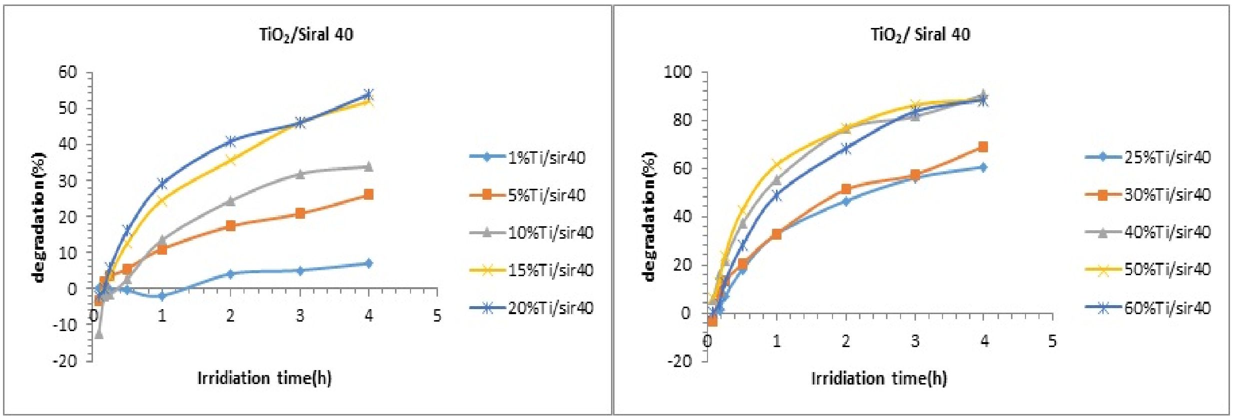

Fig. 7. Photocatalytic decomposition of 4 hours, (a) IBP over (1-25%TiO_2/Siral40) and (b) TiO_2 alone and 30-60%TiO_2/Siral40 with varying catalyst ratios. Conditions: 250 ml batch reactor, ibuprofen conc. (10 ppm), catalyst (10 mg), (4.6 W) UV/Vis, solarium bulb

In all the figures above, we noticed a gradual increase in effectiveness directly proportional to the increase of the Si ratio in Siral (20-40%) and the increase in the loading ratio of the catalyst (TiO_2) in Siral, with some exceptions; for example, 25% TiO_2 loaded in Siral 20, 30, and 40 almost arrives at 55, 65, and 60%, respectively.

Only high loading (60%) at the end of UV irradiation after 4 hours of stirring and exposure to light can come close to pure, untreated, and modified catalyst. It approaches 88.5% conversion of degradation at 60% loading of TiO_2 on Siral 20 and 30, respectively (Fig.s 5 and 6). The only positive exception is 40% TiO_2 / Sir 30. It is higher than the high loading rates of 50 and 60% sequentially, where it reaches an 86.4% conversion (Fig. 6).

Regarding the modified catalyst, 40% TiO_2 loaded on Sir40 is faster to rise to degradation of IBP to about 55% after one hour, to reach the end of the reaction cycle from irradiation for four continuous hours to about 90% (Fig. 7).

3.3. Atomic efficiency. Atomic efficiency in these photocatalytic degradations has been accounted for depending on the concentration of TiO_2 as shown in Fig. 8. The calculations have been obtained after four hours based on data taken from the photocatalytic degradation process [31].

The percentage ratio of TiO_2/Siral is affected by atomic efficiency (Figs. 8 and 9). On the other hand, the data accounted for 1 hour of treatment to compare with treatment for 4 hours to ensure the validity of the results. The treatments are repeated twice or three times. It is indicated here that atomic efficiency is calculated by Eq. 2:

$$\boldsymbol{Relative\ atomic\ efficiency} = \frac{\boldsymbol{Achieved\ deg.With\ CAT—X}\ [\%]}{\boldsymbol{Deg.by\ 100\ \%\ pure\ Catalyst}\ [\%]}\boldsymbol{X} * \boldsymbol{f} \tag{2}$$

X: concentration of TiO_2 on Siral, f =100% TiO_2.

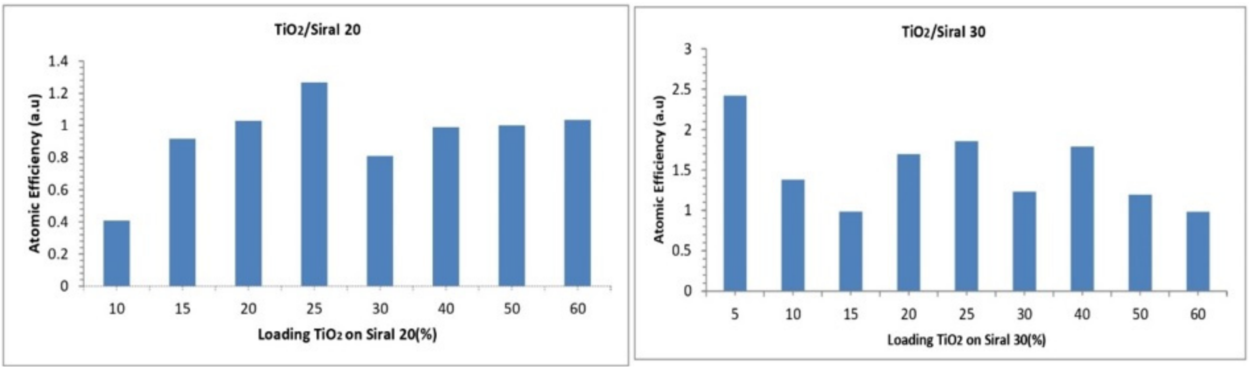

Fig. 8. Improvement of the atomic efficiency of TiO_2/Siral 20 and 30 after 4h photocatalytic treatment

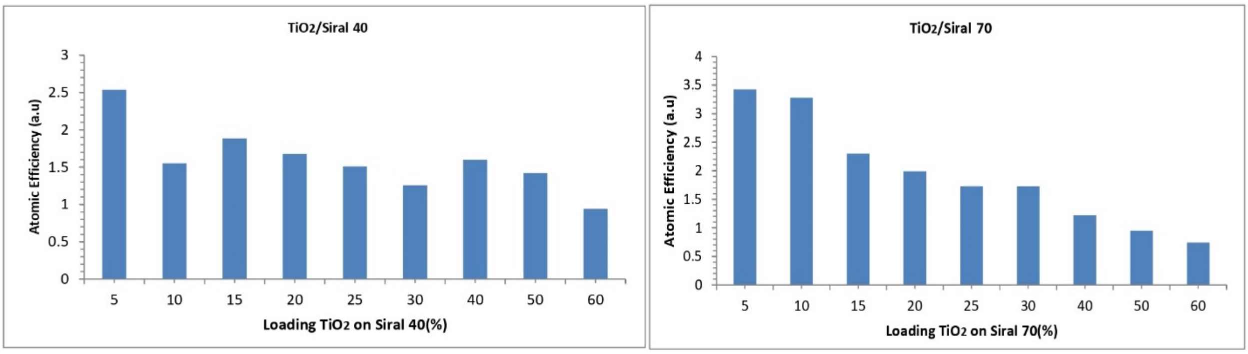

Fig. 9. Improvement of the atomic efficiency of TiO_2 / Siral 40 and 70 after 4h photocatalytic treatment

Elevated efficiency reaches a ~1.268 ratio that is computed for TiO_2/Siral20 via 25% loading of TiO_2 although a low-loading gradual increase happens until 25% loading; after that, it remains within the same range, close to 1.

With Siral 30, it becomes a bit different, as the low loading of 5% shows high efficiency achieved at 2.421; under 25% loading, the efficiency drops to 1.858. A different behavior of 2.5 is noted for TiO_2/Siral40 at 5% loading. Then there is a sort of gradual and significant decrease with the increase in the loading ratio of the catalyst until it reaches below the one at high loading, 60%. The same behavior of 3.42 and 3.28 is noted for TiO_2/Siral70 at 5 and 10% loading, respectively, followed by a noticeable and gradual decrease until it reaches 0.75 at the highest loading of 60% [32]. The Schematic illustration of the proposed photodegradation mechanism of ibuprofen over TiO_2/Siral is shown in Fig. 10.

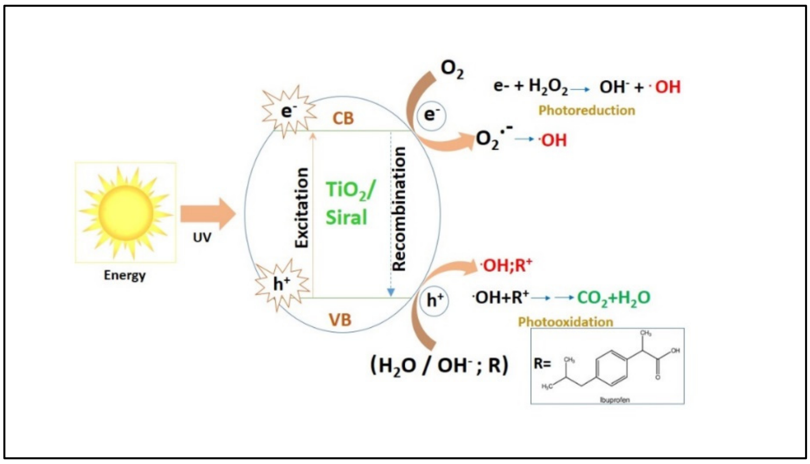

Fig. 10. Schematic illustration of the proposed photodegradation mechanism of ibuprofen over TiO_2/Siral

3.4. Nitrogen Adsorption–Desorption and Textural Properties. The surface area, pore volume, and pore size distribution of the photocatalyst were investigated using N_2 adsorption–desorption isotherms.

Table 1. Physical properties of Siral calculated from BET data [33]

Siral type	Al_2O_3/ SiO_2 %	LOI %	Loose bulk density [g/l]	Particle size (d_{50}) [µm]	Surface area (BET) [m²/g]	Pore Diameter (nm)	Pore volume [ml/g]
Siral 20	80/20	25	300-500	35	420	8.1	0.8
Siral 30	70/30	20	250-450	35	380	7.6	0.9
Siral 40	60/40	20	250-450	35	498	7.9	0.75
Siral 70	30/70	25	400-600	35	450	4.6	0.3

Irrespective of the variety of Siral series, the isotherms of adsorption and desorption of type IV N_2 are present in all samples.

Irrespective of the Siral grade, all samples exhibit type IV N_2 adsorption–desorption isotherms, characteristic of mesoporous materials. As shown in Table 1 above, the pore volume decreases progressively upon loading of the active species. Similarly, the specific surface area (S_{BET}) of the catalysts decreases for Siral 30, followed by an increase for Siral 40 and Siral 70. The average pore diameter (D_p), calculated using the Kelvin equation [34], shows a decreasing trend. This behavior is consistent with previous reports in the Ref. [35].

$$dK = \frac{-4\sigma\cos(\theta)Vm}{RTln(\frac{P}{Ps})} \qquad (3)$$

Where σ indicates surface tension, θ indicates contact angle, Vm indicates molar volume, R indicates ideal gas constant, T indicates temperature, P and Ps vapor pressure and saturated vapor respectively.

BET method and BJH correlation from the isotherm of nitrogen adsorption [36]. The surface areas have been affected by grafting; the pore diameters decrease for both Al/SiO_2 and Si/Al_2O_3. This is a result of the deposit growing orthogonal to the surface channels. Surface area, pore volume, and pore diameter of TiO_2/Siral have been reduced in most events, except in some cases, due to the loaded catalyst TiO_2 on the supports. The pore diameters and pore volumes have been decreased by loading the TiO_2 catalyst on the supports in most events [37].

Irrespective of loading the catalyst on various Siral, all treated samples illustrate type IV N_2 isotherms of adsorption and desorption, indicating that the Siral supports maintain their porosity.

When the titanium oxide loading on Siral is increased, the pore volume constantly increases. Likewise, there are decreases in BET surface areas; this is consistent with previous results in the literature of this field [38].

Table 2. Main characteristics of (TiO_2/ Siral) photocatalysts by the BET method.

Samples	**BET Surface area (m^2/g) S_{BET} (m^2/g)**	**Average Pore Diameter (n.m) DBJH (nm)**	**BJH (Vp (cm3/g)) Desorption Cumulative Pores volume (Cm^3/g)**
5% TiO_2/Sir20	326.7754	7.17906	0.71865
15% TiO_2/Sir20	304.9522	5.9463	0.69817
30% TiO_2/Sir20	219.6117	3. 9854	0.49345
60% TiO_2/Sir20	167.46965	3.1685	0.41348
5% TiO_2/Sir30	296.1029	7.43103	0.8616
15% TiO_2/Sir30	272.6285	6.24815	0.79096
30% TiO_2/Sir30	245.73985	5.8978	0.72146
60% TiO_2/Sir30	181.3864	4.72615	0.69033
5% TiO_2/Sir40	448.3685	7.40252	0.69163
15% TiO_2/Sir40	391.4702	6.89840	0.60013
30% TiO_2/Sir40	332.204	6.14531	0.54317
60% TiO_2/Sir40	198.42045	4.80961	0.41239
5% TiO_2/Sir70	355.3233	4.20467	0.27889
15% TiO_2/Sir70	272.6499	3.73701	0.22021
30% TiO_2/Sir70	214.4265	3.13749	0.18440
60% TiO_2/Sir70	118.1174	2.20718	0.09173

From Table 2, when the TiO_2 photocatalyst is applied to the Siral supports, we notice the decreasing of the surface areas, pore diameters, and pore volumes. This could be because catalyst particles have accumulated on the support surfaces. As a result of these particles entering the pores, the interior surface area is reduced. Additionally, their presence within the pores causes the pores to become smaller.

Conclusion

This study reports the successful preparation of TiO_2 nanoparticle–supported Siral nanocomposites. The presence and dispersion of TiO_2 nanoparticles on the Siral support were confirmed by UV–Vis spectroscopy and X-ray diffraction analyses. While part of the TiO_2 nanoparticles continues to grow on the external surface of the Siral framework, smaller TiO_2 particles are formed within the supercage structures. Importantly, the morphology and structural integrity of Siral remain unchanged, indicating that TiO_2 deposition does not adversely affect the support framework. The synthesized TiO_2/Siral nanocomposites exhibit excellent photocatalytic performance for the removal of ibuprofen (IBP) from contaminated water. The photocatalytic activity increases with TiO_2 loading (5–60 wt% TiO_2/Siral), demonstrating effective optimization of TiO_2 dispersion on each Siral support. This enhancement is attributed to the uniform distribution of TiO_2 nanoparticles throughout the mesoporous substrates. The formation of TiO_2 crystallites within the mesoporous Siral structure leads to a reduction in average pore diameter, pore volume, and specific surface area.

Nevertheless, these textural changes are accompanied by a significant improvement in photocatalytic efficiency. A detailed analysis of N_2 adsorption–desorption isotherms provides further insight into the relationship between TiO_2 loading, textural properties, and photocatalytic performance.

Acknowledgments. The authors are grateful to the universities of Mosul and Rostock for providing all facilities, substances, and devices.

References

1. Daniell W., Schubert U., Glöckler R., Meyer A., Noweck K., Knözinger H. Enhanced surface acidity in mixed alumina–silicas: a low-temperature FTIR study. *Applied Catalysis A: General,* 2000, **Vol .196(2)**, p. 247-260. DOI: 10.1016/S0926-860X(99)00474-3
2. Ghazal R.Y., Al-Azzawi A.G., Ali M.H. Zeolite formation using structural directing agent to enhance heavy naphtha via reforming processes. *Chemical Problems*, 2025, **Vol. 23(2)**, p. 187-201. DOI: 10.32737/2221-8688-2025-2-187-201
3. Anekwe I.M.S., Oboirien B., Isa Y.M. Effects of transition metal doping on the properties and catalytic performance of ZSM-5 zeolite catalyst on ethanol-to-hydrocarbons conversion. *Fuel Communications,* 2024, **Vol. 18**, p. 100101. DOI: 10.1016/j.jfueco.2023.100101
4. Huseynova G., Aliyeva N., Rashidova S. Zeolite-containing catalysts in alkylation processes. *Catalysis Research*, 2022, **Vol. 2(3)**, p. 1-12. DOI:10.21926/cr.2203019
5. Nifant'ev I.E., Komarov P.D., Kostomarova O.D., Kolosov N.A., Ivchenko P.V. MAO-and Borate-Free Activating Supports for Group 4 Metallocene and Post-Metallocene Catalysts of α-Olefin Polymerization and Oligomerization. *Polymers*, 2023, **Vol. 15(14)**, 3095. DOI: 10.3390/polym15143095
6. Bożęcka A., Orlof-Naturalna M., Kopeć M. Methods of dyes removal from aqueous environment. *Journal of Ecological Engineering*, 2021, **Vol. 22(9)**, DOI: 10.12911/22998993/141368
7. Gayatri R., Agustina T.E., Bahrin D., Moeksin R., Gustini G. Preparation and characterization of ZnO-zeolite nanocomposite for photocatalytic degradation by ultraviolet light. *Journal of Ecological Engineering*, 2021, **Vol. 22(2)**, p. 178-186. DOI: 10.12911/22998993/131031
8. Diban N., Pacuła A., Kumakiri I., Barquín C., Rivero M.J., Urtiaga A., Ortiz I. TiO_2–Zeolite metal composites for photocatalytic degradation of organic pollutants in water. *Catalysts,* 2021, **Vol. 11(11)**, 1367. DOI: 10.3390/catal11111367
9. Rayaroth M.P., Boczkaj G., Aubry O., Aravind U.K., Aravindakumar C.T. Advanced oxidation processes for degradation of water pollutants—ambivalent impact of carbonate species: a review. *Water,* 2023, **Vol. 15(8)**, 1615. DOI: 10.3390/w15081615
10. Alakhras F., Alhajri E., Haounati R., Ouachtak H., Addi A.A., Saleh T.A. A comparative study of photocatalytic degradation of Rhodamine B using natural-based zeolite composites. *Surfaces and Interfaces*, 2020, **Vol. 20**, 100611. DOI: 10.1016/j.surfin.2020.100611
11. Albiss B., Abu-Dalo M. Photocatalytic degradation of methylene blue using zinc oxide nanorods grown on activated carbon fibers. *Sustainability,* 2021, **Vol. 13**, 4729. DOI: 10.3390/su13094729
12. Armaković S.J., Savanović M.M., Armaković S. Titanium dioxide as the most used photocatalyst for water purification: An overview. *Catalysts,* 2022, **Vol. 13(1),** 26. DOI: 10.3390/catal13010026
13. Kocijan M., Ćurković L., Vengust D., Radošević T., Shvalya V., Gonçalves G., Podlogar M. Synergistic remediation of organic dye by titanium dioxide/reduced graphene oxide nanocomposite. *Molecules*, 2023, **Vol. 28(21)**, 7326. DOI: 10.3390/molecules28217326
14. Rubab M., Bhatti I.A., Nadeem N., Shah S.A.R., Yaseen M., Naz M.Y., Zahid M. Synthesis and photocatalytic degradation of rhodamine B using ternary zeolite/WO_3/Fe_3O_4 composite. *Nanotechnology*, 2021, **Vol. 32(34)**, 345705. DOI: 10.1088/1361-6528/ac037f
15. Stylidi M., Kondarides D.I., Verykios X.E. Pathways of solar light-induced photocatalytic degradation of azo dyes in aqueous TiO2 suspensions. *Applied Catalysis B: Environmental,* 2003, **Vol. 40(4)**, p. 271-286. DOI: 10.1016/S0926-3373(02)00163-7

16. Hama Aziz K.H., Omer K.M., Mahyar A., Miessner H., Mueller S., Moeller D., Application of photocatalytic falling film reactor to elucidate the degradation pathways of pharmaceutical diclofenac and ibuprofen in aqueous solutions. *Coatings,* 2019, **Vol. 9(8),** 465. DOI: 10.3390/coatings9080465
17. Wang Z., Srivastava V., Ambat I., Safaei Z., Sillanpää M. Degradation of Ibuprofen by UV-LED/catalytic advanced oxidation process. *Journal of Water Process Engineering,* 2019, **Vol. 31**, 100808. DOI: 10.1016/j.jwpe.2019.100808
18. Miranda M.O., Cavalcanti W.E.C., Barbosa F.F., de Sousa J.A., da Silva F.I., Pergher S.B., Braga T.P. Photocatalytic degradation of ibuprofen using titanium oxide: insights into the mechanism and preferential attack of radicals. *RSC advances*, 2021, **Vol. 11(44)**, p. 27720-27733. DOI: 10.1039/D1RA04340D
19. D'Souza J.Q., Sundaram N.G. UV induced photocatalytic degradation of caffeine using TiO_2–H-beta zeolite composite. *Minerals*, 2023, **Vol. 13(4)**, 465. DOI: 10.3390/min13040465
20. Mergenbayeva S., Abitayev Z., Batyrbayeva M., Vakros J., Mantzavinos D., Atabaev T.S., Poulopoulos S.G. TiO_2/Zeolite Composites for SMX Degradation under UV Irradiation. *Catalysts,* 2024, **Vol. 14(2)**, 147. DOI: 10.3390/catal14020147
21. Al-Azzawi A.G., Ghazal R.Y. Evaluation of Rheological and Thermal Behavior of Polymer Modified Asphalt. *Egyptian Journal of Chemistry*, 2022, **Vol. 65(11)**, p. 1-10. DOI: 10.21608/ejchem.2022.121228.5446
22. Wang Y., Wang X., Niu D., Niu Y., Xia H., Wang Y. Effect of Photocatalyst on Rheological Behavior and NO Degradation Capacity of Asphalt Binder. *Catalysts*, 2023, **Vol. 13(7)**, 1083. DOI: 10.3390/catal13071083
23. Ibrahim M.W., Khane Y., Mahmood Y.T., Schulz A., Kosslick H. Mesoporous Aluminosilicate Zinc Oxide Photocatalytic Degradation of Pharmaceutical Pollutants. *Desalination and Water Treatment*, 2024, **Vol. 320**, 100588. DOI: 10.1016/j.dwt.2024.100588
24. Al-Azzawi A.G., Iraqi A., Aziz S.B., Zhang Y., Murad A.R., Hadi J.M., Lidzey D.G. Synthesis, optical and electrochemical properties of naphthothiadiazole-based donor-acceptor polymers and their photovoltaic applications. *International Journal of Electrochemical Science*, 2021, **Vol. 16(12)**, 21125. DOI: 10.20964/2021.12.32
25. Gonzalez-Burciaga L., Nunez-Nunez C., Morones-Esquivel M., Avila-Santos M., Lemus-Santana A., Proal-Najera J. Characterization and Comparative Performance of TiO_2 Photocatalysts on 6-Mercaptopurine Degradation by Solar Heterogeneous Photocatalysis. *Catalysts.* 2020*,* **Vol. 10,** 118. DOI: 10.3390/catal10010118
26. Nasiri S., Rabiei M., Palevicius A., Janusas G., Vilkauskas A., Nutalapati V., Monshi A. Modified Scherrer equation to calculate crystal size by XRD with high accuracy, examples Fe_2O_3, TiO_2 and V_2O_5. *Nano Trends*, 2023, **Vol. 3**, 100015. DOI: 10.1016/j.nwnano.2023.100015
27. Uddin M.J., Cesano F., Chowdhury A.R., Trad T., Cravanzola S., Martra G., Lorenzo M., Adriano Z., Scarano D. Surface structure and phase composition of TiO_2 P25 particles after thermal treatments and HF etching. *Frontiers in Materials*, 2020, **Vol. 7**, 192. DOI: 10.3389/fmats.2020.00192
28. Chen Y.-J., Lin T.-S. Enhancement of visible-light photocatalytic efficiency of TiO_2 nanopowder by anatase/rutile dual phase formation. *Applied Sciences*, 2020. **Vol. 10(18)**, 6353. DOI: 10.3390/app10186353
29. Keiteb A.S., Saion E., Zakaria A., Soltani N., Abdullahi N. A modified thermal treatment method for the up-scalable synthesis of size-controlled nanocrystalline titania. *Applied Sciences*, 2016, **Vol. 6(10)**, 295. DOI: 10.3390/app6100295
30. Ohtani B., Prieto-Mahaney O., Li D., Abe R. What is Degussa (Evonik) P25? Crystalline composition analysis, reconstruction from isolated pure particles and photocatalytic activity test. *Journal of Photochemistry and Photobiology A: Chemistry,* 2010, **Vol. 216(2-3)**, p. 179-182. DOI: 10.1016/j.jphotochem.2010.07.024

31. Ibrahim M.W., Khane Y., Mahmood Y.T., Schulz A., Kosslick H. Mesoporous aluminosilicate materials supported zinc oxide photocatalytic degradation of pharmaceutical pollutants. *Desalination and Water Treatment*, 2024, **Vol. 320**, 100588. DOI: 10.1016/j.dwt.2024.100588
32. Braz F.S., Silva M.R., Silva F.S., Andrade S.J., Fonseca A.L., Kondo M.M. Photocatalytic degradation of ibuprofen using TiO_2 and ecotoxicological assessment of degradation intermediates against Daphnia similis. *Journal of Environmental Protection*, 2014, **Vol. 5(7),** p. 620-626. DOI: 10.4236/jep.2014.57063
33. Masthan S.K. Study of the influence of alumina content on pore structure stability of synthetic silica-alumina catalysts. *Indian Journal of Chemistry*, 1995, **Vol. 34A,** p. 213-215. DOI: 10.1007/s10934-015-0101-z
34. Tsuru T., Takata Y., Kondo H., Hirano F., Yoshioka T., Asaeda M. Characterization od sol-gel derived membranes and zeolite membranes by nanopermporometry. *Separation and Purification Technology,* 2003, **Vol. 32(1-3),** p. 23-27. DOI: 10.1016/S1383-5866(03)00036-4
35. Raj K., Viswanathan B. Effect of surface area, pore volume and particle size of P25 titania on the phase transformation of anatase to rutile. *Indian Journal of Chemistry,* 2009, **Vol. 48A**, p. 1378-1382.
36. Chen C., Salinger J.L., Essig M.E., Walton I.M., Fulvio P.F., Walton K.S. Hierarchical Silica Composites for Enhanced Water Adsorption at Low Humidity. *ACS Applied Materials & Interfaces,* 2024, **Vol. 16(30)**, p. 40275-40285. DOI: 10.1021/acsami.4c09456
37. Khalil M.I., Ayed N.J., Ghazal R.Y. Preparation of Nickel-Grafted Zeolite From a Local Mineral Ore and Studying Their Catalytic Properties. *Macromolecular Symposia,* 2025, **Vol. 414,** 2400221. DOI: 10.1002/masy.202400221
38. Petcu G., Papa F., Anghel E.M., Atkinson I., Preda S., Somacescu S., Daniela C.C., Adriana B., Elena M.C., Mariana C., Viorica P., Jecu L.M. Effects of Aluminosilicate Gel Treatment and TiO_2 Loading on Photocatalytic Properties of Au–TiO_2/Zeolite Y. *Gels,* 2023, **Vol. 9(6)**, 503. DOI: 10.3390/gels9060503